Citation: Zhan, M. J., X. C. Li, H. M. Sun, et al., 2018: Changes of extreme maximum temperature events and population exposure in China under global warming of 1.5 and 2.0 ℃: Analysis using a regional climate model COSMO−CLM. *J. Meteor. Res.*, **32**(1), XXX-XXX, doi: 10.1007/s13351-018-7016-y. (in press)

Changes of Extreme Maximum Temperature Events and Population Exposure in China under Global Warming of 1.5 and 2.0 ℃:: Analysis using a Regional Climate Model COSMO–CLM

Mingjin ZHAN（占明锦）[1,4,5], Xiucang LI（李修仓）[2,3], Hemin SUN（孙赫敏）[2], Jianqing ZHAI（翟建青）[3], Tong JIANG（姜彤）[3], and Yanjun WANG（王艳君）[2*]

1 *Chinese Academy of Meteorological Sciences, Beijing* 100081

2 *Collaborative Innovation Center on Forecast and Evaluation of Meteorological Disasters, School of Geography and Remote Sensing, Nanjing University of Information Science & Technology, Nanjing* 210044

3 *National Climate Center, China Meteorological Administration, Beijing* 100081

4 *University of the Chinese Academy of Sciences, Beijing* 100049

5 *Jiangxi Provincial Climate Centre, Nanchang* 330046

(Received February 04, 2017; in final form September 17, 2017)

Supported by the National Natural Science Foundation of China (41571494, 41661144027, and 41671211).

* Corresponding author: yjwang78@163.com.

ABSTRACT

Based on daily maximum temperature data (1986–2100) from the COSMO–CLM regional climate model and population statistics of China for 2010, and by using the Intensity–Area–Duration (IAD) method, the frequency, intensity, coverage, and population exposure of extreme maximum temperature events (EMTEs) are determined. Between 1986 and 2005 (reference period), the frequency, intensity, and coverage of EMTEs are 1330–1680 times /a, 31.4–33.3 ℃, and 1.76–3.88 million km^2, respectively. The center of the most severe EMTEs is located in central China, and 179.5–392.8 million people are exposed to EMTEs annually. The findings in relation to the 1.5 and 2.0 ℃ global warming scenarios are as follows. 1) Relative to 1986-2005, under 1.5 ℃ warming, the frequency, intensity, and coverage increase by 1.13%–6.84%, 0.32%–1.50%, and 15.98%–30.68%, whereas under 2.0 ℃ warming, the increases are 1.73%–12.48%, 0.64%–2.76%, and 31.96%–50.00%, respectively. 2) It is possible that both the intensity and coverage of future EMTEs could exceed the most severe observed EMTEs. In addition, two new centers of EMTEs are projected to develop under 1.5 ℃ warming: one in North China and the other in Southwest China. Under 2.0 ℃ warming, a fourth EMTE center is projected to develop in Northwest China. 3) Under 1.5 and 2.0 ℃ warming, population exposure is projected to increase by 23.2%–39.2% and 26.6%–48%. From a regional perspective, the population exposure is expected to increase fastest in Southwest China. A greater proportion of the population in North, Northeast, and Northwest China will be

exposed to EMTEs under 2.0 ℃ warming. The results show that a warming world will lead to increases in the intensity, frequency, and coverage of EMTEs. Furthermore, 2.0 ℃ warming will lead to both more severe EMTEs and more people exposed. Given the probability of the increased occurrence of EMTEs more severe than in the past, it is vitally important to China that the global temperature increase be limited to 1.5 ℃.

Key words: extreme maximum temperature events (EMTEs), population exposure, 1.5 and 2.0 ℃ global warming, COSMO–CLM regional climate model, China

1. Introduction

Over recent centuries, an increase in global mean surface temperature has been observed. Between 1986 and 2005, the global mean surface temperature has risen more than 0.61 ℃ above pre–industrial levels (1850–1900) (IPCC, 2013). Under this trend of global warming, extreme events such as heat waves have shown many new characteristics in terms of frequency, intensity, impact range, and duration (Field et al., 2012). On December 12, 2015, the Paris Agreement was negotiated by representatives of 195 countries at the 21st Conference of the Parties of the UNFCCC in Paris, and adopted by consensus. The stated aim of the Paris Agreement (UNFCCC, 2015) is "Holding the increase in the global average temperature to well below 2.0 ℃ above pre–industrial levels and to pursue efforts to limit the temperature increase to 1.5 ℃ above pre–industrial levels, recognizing that this would significantly reduce the risks and impacts of climate change." The adoption of the Paris Agreement reflects the historic importance of the global cooperation pledged to address future climate change.

With global warming, the characteristics of extreme maximum temperature and extreme maximum temperature events (EMTEs) have changed globally and in China. Since the middle of the 20th century, there has been a likely increasing trend in the frequency of heat waves in Europe, Australia and across much of Asia. Globally, there is medium confidence owing to lack of studies over Africa and South America (Easterling et al., 2005; Hansen et al., 2006; IPCC, 2013; Perkins et al., 2012). The latest HadGHCND (Hadley Centre Global Historical Climatology Network Daily) database indicates that global trends in observed heat waves are increasing in intensity, frequency, and duration (Perkins et al., 2012). In different regions of the world, the maximum temperature has shown a significant upward trend since the latter part of the 20^{th} century (Kothawale and Kumar, 2005; Kousari et al., 2013; Homar et al., 2010; Kruger and Sekele, 2013). Globally, 41.0% of the land area has experienced a significant increase in the annual occurrence of warm days (TX90p in days decade−1), and 28.8% of the land area has experienced an increase in warm spell duration (Alexander et al., 2006). For most of China, the trend of rise in air temperature has been increasing more rapidly since the 1980s (Shi et al., 2003). From a regional perspective, the characteristics of high temperatures are very complex. Both the numbers of days and the intensities of EMTEs have increased significantly over the southeastern coast and northern areas of China, with a dramatically increasing trend since the 1990s. However, significant negative trends have been detected in the lower reaches of the Yellow River and to the north of the Yangtze River (Ding et al., 2007; Xu et al., 2009; Ding et al., 2010). Overall, significant positive trends in the frequencies of EMTEs prevail in most of China.

Changes in EMTEs are an important aspect of climate change because their effects on natural ecosystems and human society can be more profound than mean temperature change (Karl and Easterling, 1999; Easterling et al., 2000; Upperman et al., 2015). In recent years, EMTEs have affected many parts of the world. Such events are the most prominent cause of weather–related human mortality in the U.S. (National Center for Health Statistics, 2007; National Weather Service, 2009), and they are responsible for more deaths annually than hurricanes, lightning, tornadoes, floods, and earthquakes combined (Greene et al., 2011). Record–breaking EMTEs occurred in Europe in summer 2003, and it has been suggested they were responsible for an estimated 40,000 deaths across central and western parts of the continent (Valleron and Boumendil, 2004). In 2013, a large–scale EMTE persisted across China. During this event, 57, 49, and 47 hot days (daily maximum temperature ≥ 35 °C) were recorded in Changsha, Chongqing, and Hangzhou, respectively, with the highest daily temperature of 38.2, 40.9, and 40.5 ℃, respectively. This EMTE in 2013 cost 83.56 billion RMB in direct economic losses nationwide (China Meteorological Administration, 2013). Following this historic heat wave disaster in 2013, public concern has led to an increase in research into the EMTEs. In order to mitigate the negative impacts of EMTEs, we should not focus solely on the past but also pay attention to future climate change and to its impacts.

Climate models, including Global Climate models (GCMs) and Regional Climate models (RCMs), are used widely as basic tools for past climate simulation and future climate projections. At a global scale, the Inter–Sectoral Impact Model Intercomparison Project (ISI–MIP) has been used to perform a series of climate change impact studies by driven GCMs (Dankers et al., 2013; Davie et al., 2013; Ito et al., 2016). At the regional scale, the resolution of GCMs is too low to support the climate change impact studies. Statistical downscaling can be used to improve the resolution of GCMs, but physical mechanisms and dynamical processes are ignored. Based on dynamical downscaling, the RCMs would be better for capturing extremes with high resolution in regions of complex topography and land–surface processes. The COSMO–CLM (CCLM) regional climate model is developed from the Local Model (LM) of the German Meteorological Office, and it has been used for simulations of temperature and rainfall in some Chinese regions, e.g., the Tarim River Basin, Yangtze River Basin, Huaihe River Basin, and Pearl River Basin (Gemmer et al., 2008; Tan et al., 2012; Cao et al., 2013; Fischer et al., 2013; Wang et al., 2013). In this study, the projected daily maximum temperature data under RCP 2.6 and RCP 4.5 scenarios from the CCLM for 1961–2100 in China will be used.

Research of extreme climate events has developed from value analysis at a single site (Wang and Yang , 2007; Zhang et al., 2008) to related investigations of intensity, impact range, and duration (Jing et al., 2016; Zhai et al., 2017). Based on the intensity–area–duration (IAD) method, Zhai et al. (2017) developed an approach for identifying a regional extreme event and for analyzing its coverage and duration. Using daily precipitation data from 771 stations from 1960 to 2014, Jing et al. (2016) produced distribution patterns of the trend of change of regional extreme precipitation events in China and they discussed the exposure of the population and economy.

This study projects the changes of EMTEs (frequency, intensity, impact area) under the 1.5 and 2.0 ℃ global warming scenarios in China, based on the CCLM outputs. Combined with the demographic data in 2010, population exposure to EMTEs in China in the warming world will be assessed. The main target of this study is to project the influence and characteristics of the EMTEs under the 1.5 and 2.0 ℃ global warming scenarios, to provide evidence of the impacts expected from an extra increase of 0.5 ℃ to support policymakers in the development of climate change mitigation strategies.

2. Data

2.1 Observed data

Quality–controlled daily maximum temperature datasets are issued by the National Meteorological Information Center of the China Meteorological Administration. These datasets for 756 meteorological stations throughout China start from January 1, 1961 and end on December 31, 2015 (Fig. 1).The rate of missing daily maximum temperature data in these datasets is <0.25% annually; thus, the observed data can be used to reflect the spatiotemporal distribution of daily maximum temperature in China.

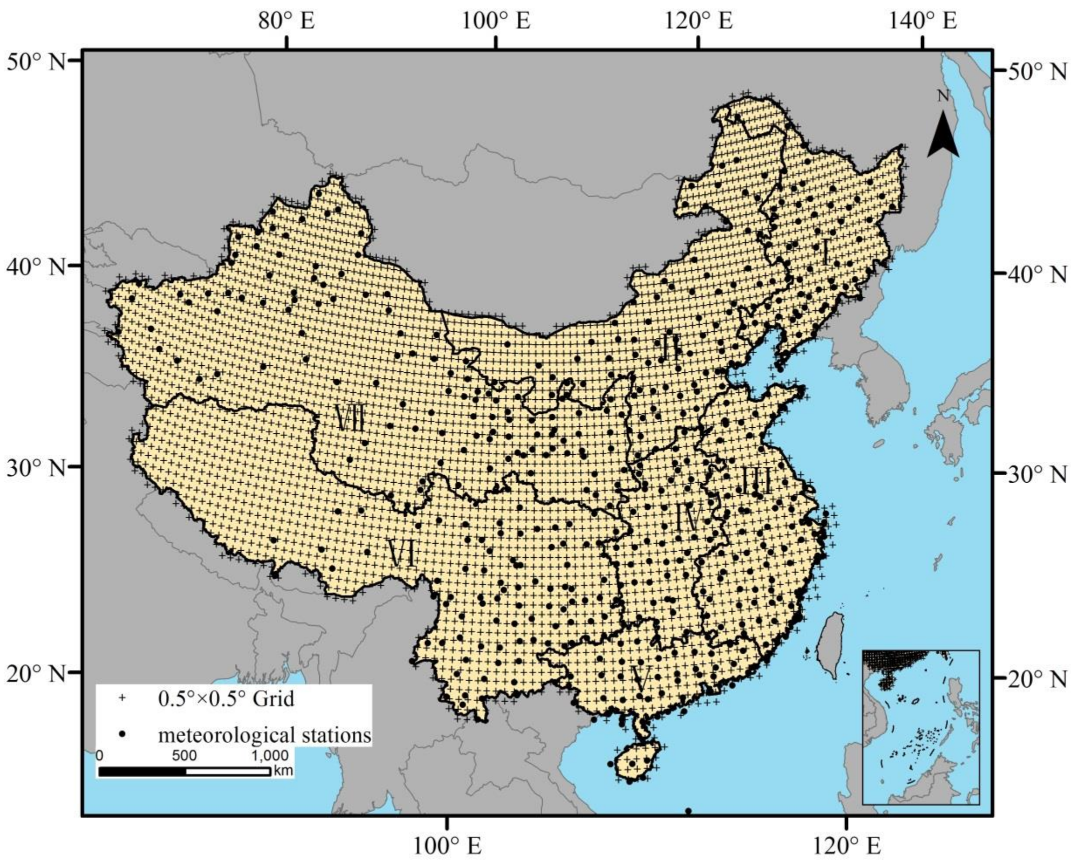

Fig. 1. Spatial distribution of meteorological stations and the CCLM grid of China.

To study the exposure of the population of China to EMTEs, the country was divided into seven geographic areas: I Northeast China, II North China, III East China, IV Central China, V South China, VI Southwest China, and VII Northwest China (Fig. 2). The population distribution data were obtained from the Sixth Nationwide Population Census (National Bureau of Statistics of the People’s Republic of China, 2010). The population of China is concentrated mainly in four of the geographic areas:

North (Beijing–Tianjin–Hebei Metropolitan Region), Central (Yangtze River Delta Urban Agglomeration), South (Pearl River Delta Urban Agglomeration), and Southwest (Chongqing–Sichuan Region). The population density in the Northeast and Northwest areas is relatively lower (Fig. 2).

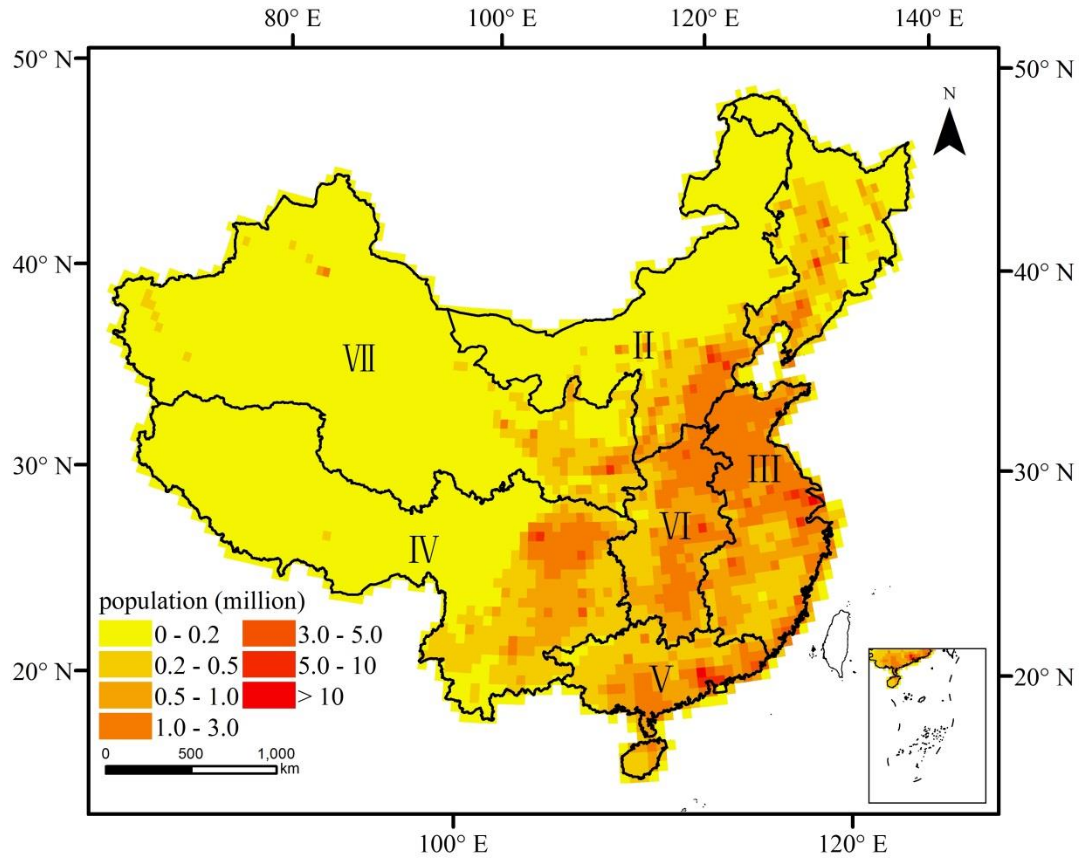

Fig. 2. Spatial distribution of population of China in 2010.

2.2 CCLM data

The CCLM regional climate model is the climate version of the operational weather forecasting model of the Consortium for Small–scale Modeling (COSMO, http://cosmo–model.org), which has been adapted and developed as a tool to project future changes in climate parameters (Burkhard et al., 2008; Fischer et al., 2013; Cao et al., 2013; Huang et al., 2015; Su et al., 2016). The CCLM is a nonhydrostatic regional climate model (Steppeler et al., 2003) intended for spatial resolutions of meso–b and meso–c scale, where nonhydrostatic effects begin to have an important role in the evolution of atmospheric flows. It belongs to a dynamical regional climate model based on primitive thermohydrodynamical equations used to describe the atmospheric circulation at resolutions of 1–50 km (Huang et al., 2017a).

In this study, daily maximum temperature data from the COSMO–CLM (CCLM) model were obtained from the Potsdam Institute for Climate Impact Research in Germany. With spatial resolution of 0.44°, the CCLM output was transferred to a regular 0.5° resolution grid using a bilinear interpolation method (Huang et al., 2015), which generated a total of 4063 grids that covered China. Changes in the characteristics of EMTEs under global warming scenarios of 1.5 and 2.0 ℃ (relative to pre–industrial levels) were analyzed by comparing them with the reference period of 1986–2005.

2.3 Validation of CCLM

The simulation capability of the CCLM in terms of daily maximum temperature in China for 1986–2005 can be assessed by comparison of Figs. 3, 4.

Figure 3 illustrates the spatial distribution of observed and simulated daily maximum temperature in China. From Figs. 3a, b, it can be seen that the daily maximum temperature in East China decreases from south to north, while in West China, it decreases from north to south because of the complex terrain effects. Large–value centers, locating mainly in the southern coastal region (Guangdong, Guangxi, and Hainan provinces), southwest region (Sichuan province) and northwest region (Xinjiang Province), and low–value centers, locating mainly in the northeast (Heilongjiang Province) and southwest (Sichuan and Qinghai provinces), are simulated very well. Totally, the spatial correlation coefficient between the observed and simulated temperatures is 0.90, significant at the 5% level. Therefore, it is evident that the CCLM is able to capture well the spatial distribution of daily maximum temperature in China.

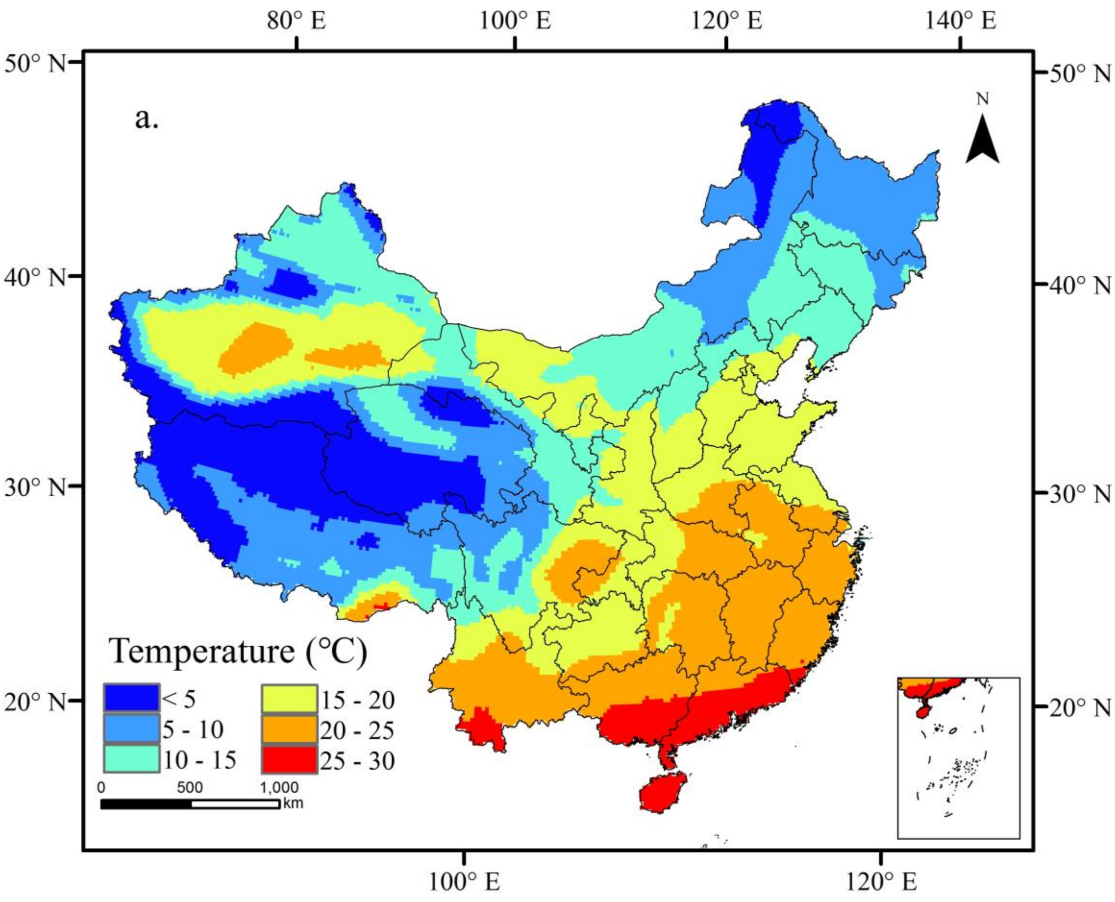

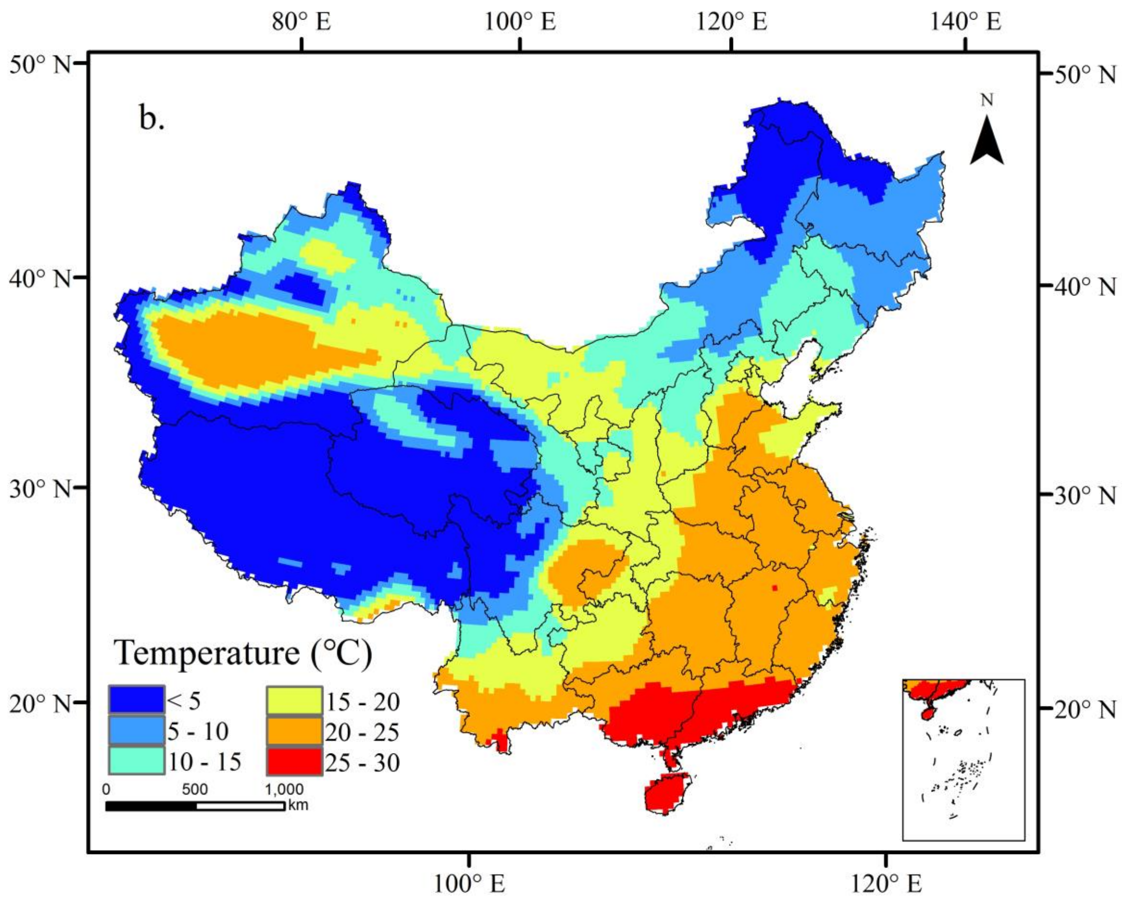

Fig. 3. Spatial distribution of annual mean daily maximum temperature (1986–2005): (a) observed and (b) simulated.

Figure 4 illustrates the temporal variation of the observed and CCLM annual maximum temperature data from 1986 to 2005. In general, the CCLM data are systemic lower than the observed, although both time series exhibit similar increasing trends. The rates of increase of the observed and simulated data are 0.16 and 0.28 ℃/decade, respectively, significant at the 5% level. Based on a Taylor diagram (Taylor, 2001, Fig.5), the correlation coefficient is 0.73 and the root–mean–square deviation is 0.39. Overall, the CCLM is shown capable of simulating daily maximum temperature at station level for 1986–2005, indicating that the simulation data are suitable for the analysis of the spatiotemporal variation of EMTEs.

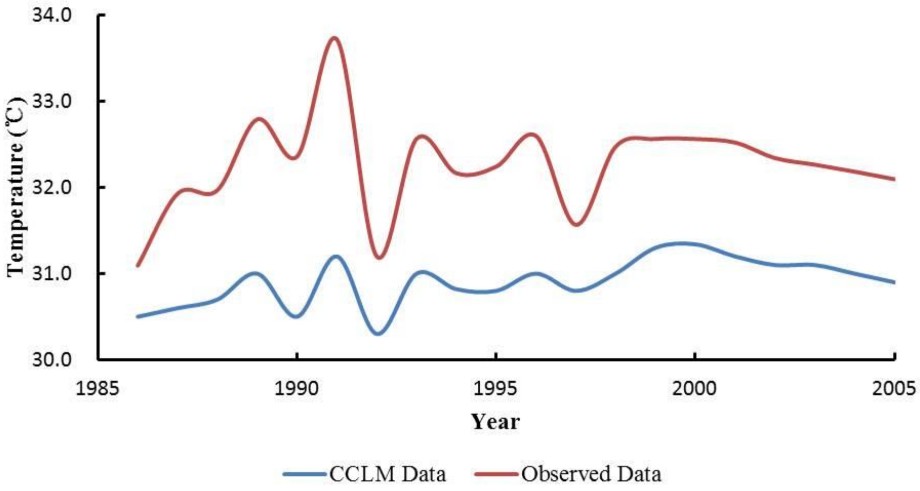

Fig. 4. Temporal variation of annual mean daily maximum temperature, 1986–2005.

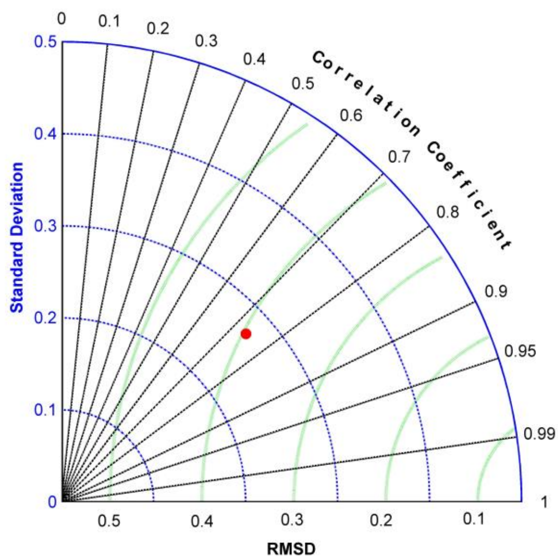

Fig. 5. Annual maximum temperature Taylor diagrams of CCLM.

3. Method

3.1 Identification of EMTEs

Extreme temperature events are often described by different standards. In China, it is common for a daily maximum temperature of 35 ℃ to be considered an extreme high temperature (Zhang et al., 2004). However, considering the large area of Northeast China and the impact on human health, a temperature of 30 ℃ is selected as the threshold of EMTEs (Vescovi et al., 2009).

In most previous studies, the characteristics of EMTEs have been analyzed at station– or grid–scale (Zhou & Ren, 2011; Qin et al., 2015) and they have failed to consider the temporal and spatial continuity of EMTEs. In this study, the EMTEs were identified using the IAD method (Andreadis et al., 2005; Sheffield et al., 2009), taking high temperature intensity, coverage and duration characteristics (1–day, 3–day and 5–day) into account. This method has already been applied successfully in drought and extreme precipitation analyses in China (Chen et al., 2016; Jing et al., 2016; Huang et al., 2017b; Zhai et al., 2017).

The principle of the IAD method is to identify grids that neighbor the maximum high temperature center and then to cluster the grids with the high temperature ⩾30 ℃ into an event. The coverage is determined as the summation of all grids, and the intensity is determined as the average of the temperature of all grids included in one event, as illustrated in Fig. 6. For example, Fig.6 shows two EMTEs in Area a. Event 1 is in the blue grid and Event 2 in the red grid. From the IAD curve Event 1 (dotted blue line), we find the impact area of Event 1 is 4×10^4 km^2, the intensity is 33.5 ℃ (the average of the four grids), and the maximum intensity is 38 ℃. The highest intensity at a contiguous impact area is presented by the IAD envelope curve (Fig. 6, solid black line). While the IAD curve can be used to compare EMTEs of different intensity and area, the IAD envelope curve identifies the highest intensity at each contiguous impact area for the entire study period. Further more details about IAD method can be found in Zhai et al. (2017).

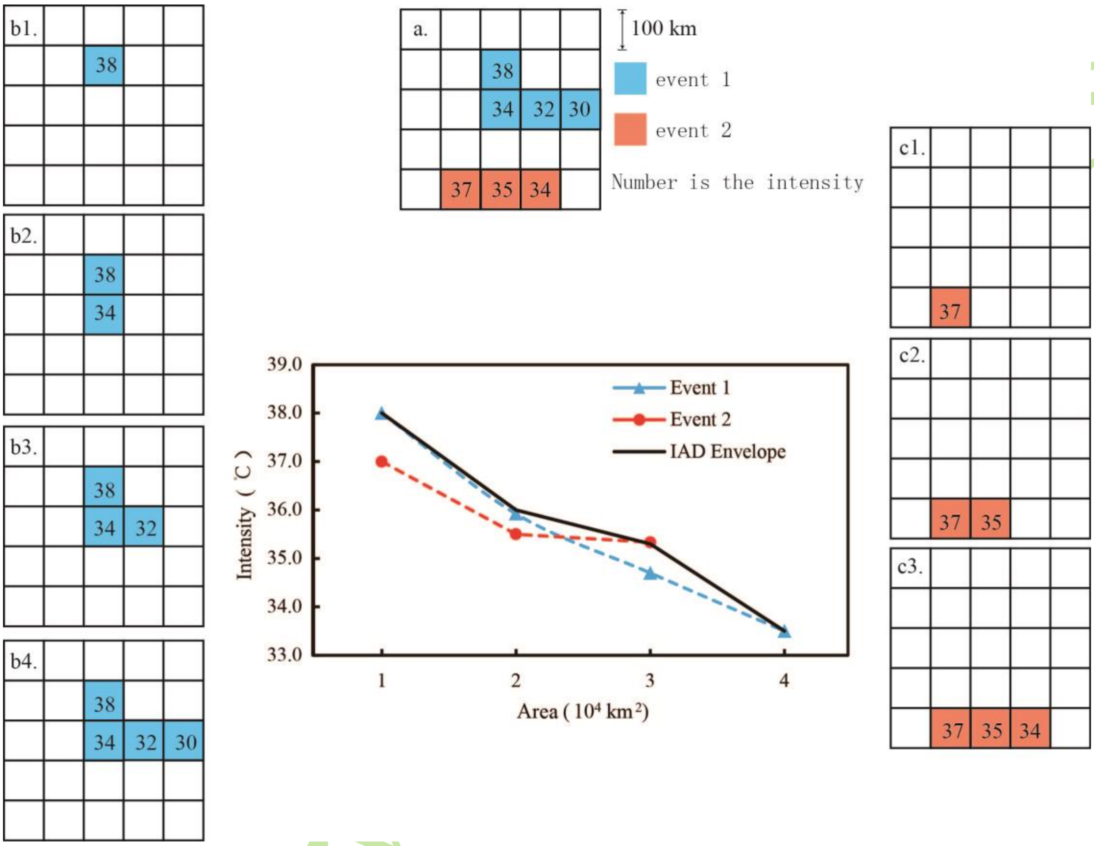

Fig. 6. Construction of the IAD curve and IAD envelope curve.

3.2 Time horizons of 1.5 and 2.0 ℃ global warming thresholds

Global temperatures observed during 1986–2005 were 0.61 ℃ higher than pre–industrial levels (1850–1900) (IPCC, 2013). Therefore, to reach a global temperature increase of 1.5 and 2.0 ℃ means the temperature has to increase by a further 0.89 and 1.39 ℃, respectively. The Representative Concentration Pathway (RCP) 2.6 refers to mitigation scenarios intended to restrict the increase of global mean temperature to 1.5 ℃ during the 21st century. The RCP4.5 is a scenario that stabilizes radiative forcing at 4.5 W m^{-2} by 2100; thus, limiting the global means temperature increase to 2.0 ℃ (Rogeljet al., 2011; Thomson et al., 2011; Vuuren et al., 2011).

Because the results obtained from a single climate model could have large uncertainty, this study used six GCMs: GFDL, HAD, IPSL, MIROC, NOR and MPI–ESM–LR to determine when the global mean temperature will be 1.5 and 2.0 ℃ warmer. The ensemble data in Fig. 7 suggest that the global mean temperature will surpasses the 1.5 ℃ threshold after 2030 under RCP2.6. Under RCP4.5, the ensemble data suggest that the global mean temperature will exceed the 2.0 ℃ warming threshold after 2049. Considering the comparatively stable climate condition, a 20–yr running average of 2030 (2020–2039) and 2049 (2040–2059) are set as the 1.5 and 2.0 ℃ warming period, respectively (Frieler et al., 2016; Warszawski et al., 2014).

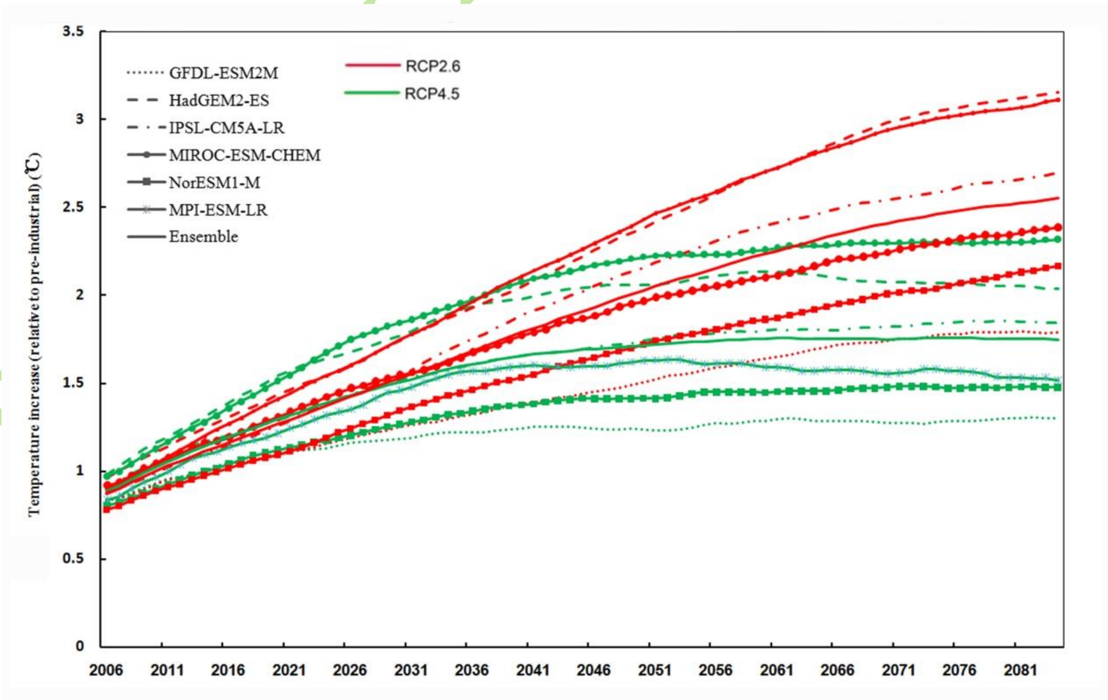

Fig. 7. Mean global surface temperature (2006–2100) relative to the pre–industrial period projected by ensembles of Global Climate Models (GCMs).

4. Results

4.1 Changes in EMTEs

4.1.1 Frequency of EMTEs

Figure 8 illustrates the projected frequencies of EMTEs under 1.5 and 2.0 ℃ warming. Relative to the reference period (1680 times/a), the frequency of 1–day events for 1.5 ℃ warming is 1699 times/a, an increase of 1.13%; under 2.0 ℃ warming, the frequency increases by 1.73% to 1709 times/a. Under global warming of 1.5 and 2.0 ℃, the frequency of 3–day events increases by 3.83% (1547 times/a) and 6.55% (1595 times/a), respectively, relative to the reference period, and the frequency of 5–day events increases by 6.84% (1421 times/a) and 12.48% (1496 times/a), respectively. Based on a student's t–test, relative to the reference period, the increase in frequency is significant under 2.0 ℃ world ($p \leq 0.05$) but not significant under 1.5 ℃ warming. Overall, global warming of 2.0 ℃ shows an even greater increase than that of 1.5 ℃, and the frequency of 5–day events shows the greatest growth. Therefore, a warmer world will mean EMTEs will become more frequent and have longer durations.

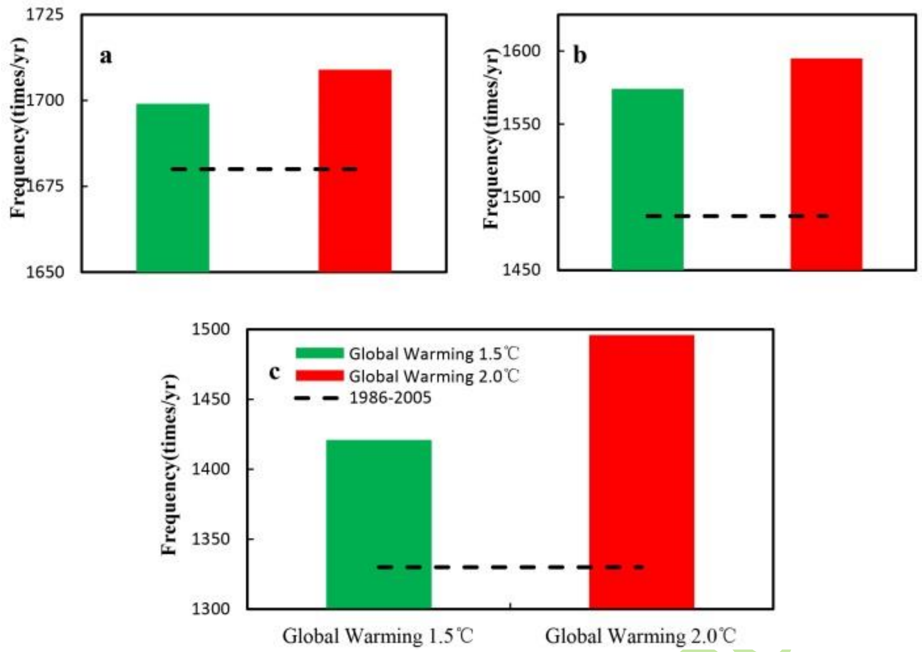

Fig. 8. Frequency of EMTEs under 1.5 and 2.0 ℃ global warming (duration: a, 1–day; b, 3–day; c, 5–day).

4.1.2 Intensity of EMTEs

The projected changes in intensity of EMTEs are shown in Fig. 9. The average intensity of 1–day EMTEs is 31.4 ℃ (reference period), 31.5 ℃ (1.5 ℃ warming), and 31.6 ℃ (2.0 ℃ warming), increases of 0.32% and 0.64%, respectively for the warming scenarios. The average intensity of 3–day EMTEs is 32.6 ℃ (reference period) with increases of 1.23% (33.0 ℃) and 2.76% (33.5 ℃) for global warming of 1.5 and 2.0 ℃, respectively. The average intensity of 5–day EMTEs is 33.3, 33.8, and 34.0 ℃ for the reference period, and the 1.5 and 2.0 ℃ warming scenarios, respectively. The increases relative to the reference period for the 1.5 and 2 ℃ warming scenarios are 1.50% and 2.10%, respectively. Irrespective of duration, the intensity increases significantly under both warming scenarios ($p \leq 0.05$).

Compared with 1.5 ℃ warming, the intensities of EMTEs will increase by 0.32%–1.51% under 2.0 ℃ warming. In general, in a warmer world, the intensity of EMTEs will become stronger.

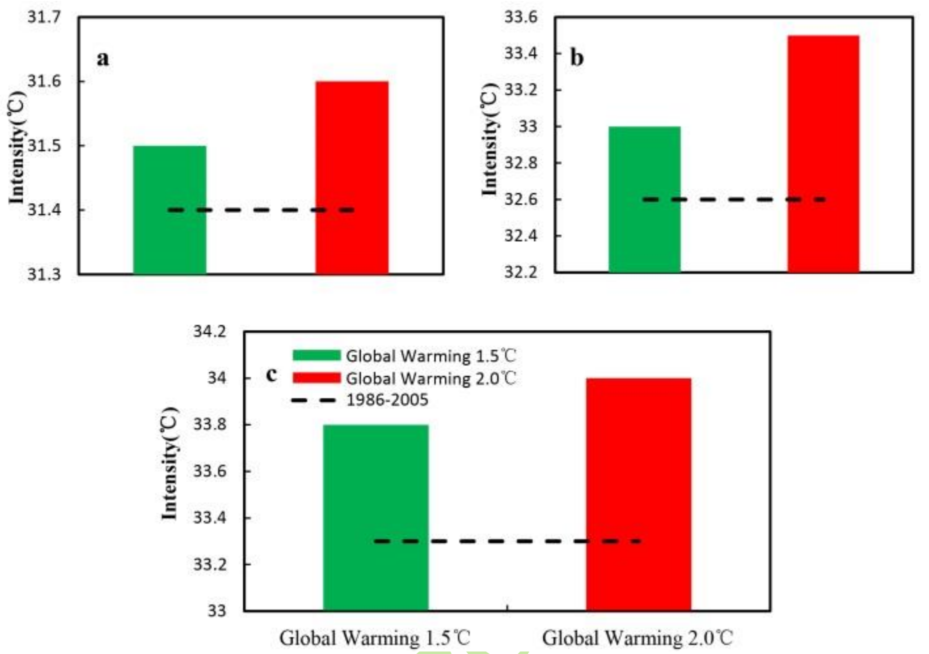

Fig. 9. Intensity of EMTEs under 1.5 ℃ and 2.0 ℃ global warming (duration: a, 1–day; b, 3–day; c, 5–day).

4.1.3 Coverage of EMTEs

The changes in projected annual coverage of EMTEs are illustrated in Fig. 10. The area of annual coverage of 1–day EMTEs is 4.60 million km^2 for global warming of 1.5 ℃ and 5.12 million km^2 for 2.0 ℃; increases of 15.98% and 31.96%, respectively, relative to the reference period (3.88 million km^2). For 3–day EMTEs, the area of annual coverage is 3.10 million km^2 for 1.5 ℃ global warming and 3.51 million km^2 for 2.0 ℃; increases of 25.00% and 41.53%, respectively, relative to the reference period (2.48 million km^2). For 5–day extreme events, the area of annual coverage is 2.30 million km^2 for 1.5 ℃ global warming and 2.64 million km^2 for

2.0 ℃ warming; increases of 30.68% and 50.00%, respectively, relative to the reference period (1.76 million km^2). The increase in coverage is significant ($p \leq 0.05$) under both warming scenarios.

Compared with 1.5 ℃ warming, the coverage of EMTEs will increase significantly by 13.22%–23.07% under 2.0 ℃ warming ($p \leq 0.05$). The coverage of EMTEs under 2.0 ℃ warming is the largest. It is worth noting that the rates of increase of 3– and 5–day events under 1.5 and 2.0 ℃ warming are greater than the rate of increase of 1–day event, and that the rate of increase of 5–day events is the largest. This means that in a warmer future, longer–lasting EMTEs might account for a greater proportion of the overall coverage.

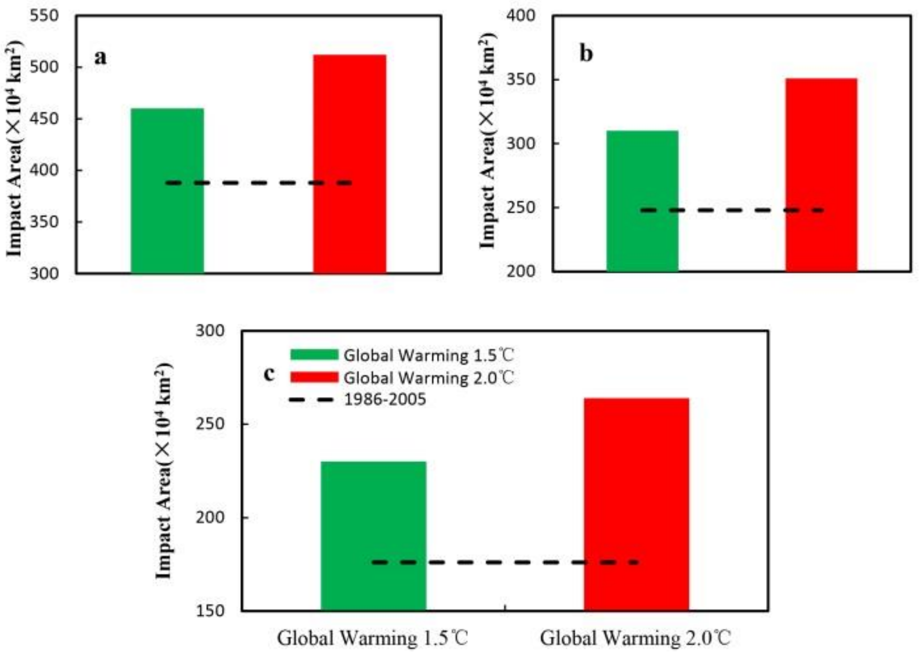

Fig.10. Annual coverage of EMTEs under 1.5 ℃ and 2.0 ℃ global warming (duration: a, 1–day; b, 3–day; c, 5–day).

4.1.4 Changes in the strongest EMTEs

The envelopes shown in Fig. 11 encompass the strongest EMTEs. Comparing the EMTEs and envelopes of the 1.5 and 2.0 ℃ warming scenarios with the envelope of the reference period shows whether the EMTEs under the two global warming scenarios are stronger than the strongest events in the reference period. Under 1.5 ℃ warming, there are 10 1–day EMTEs outside the envelope. These events have greater intensity for the same coverage or larger coverage for the same intensity. Under 2.0 ℃ warming, there are 26 1–day EMTEs outside the envelope. Similarly, there are 24 and 72 3–day EMTEs and 20 and 28 5–day EMTEs outside the envelopes for global warming of 1.5 and 2.0 ℃, respectively. The envelopes for global warming of 1.5 ℃ (green) and of 2.0 ℃ (red) both lie above the envelope of the reference period (black solid line), irrespective of whether for 1–, 3–, or 5–day EMTEs (Fig. 9).

To summarize, in a warming world (either 1.5 or 2.0 ℃ scenario), some (1–, 3–, and 5–day EMTEs) might exceed the severest events in the reference period. Furthermore, greater warming means a higher probability of EMTEs. The intensity of the most severe EMTEs under 2.0 ℃ warming will be stronger than EMTEs with similar coverage under 1.5 ℃ warming.

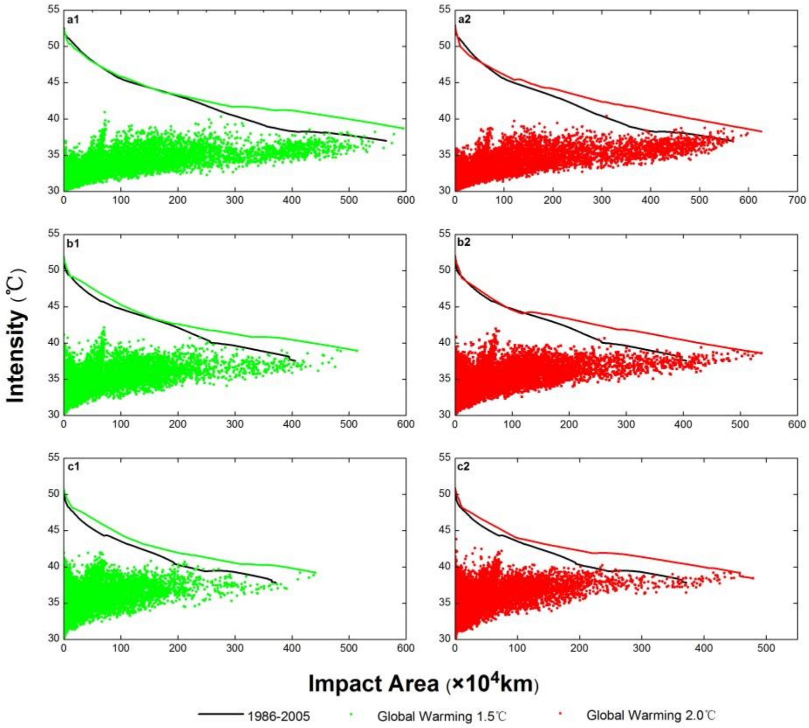

Fig.11. Comparison of EMTEs under the global warming of 1.5 and 2.0 ℃ with the baseline period IAD , Global Warming 1.5 and Global Warming 2.0 ℃ envelope (a1–a2, EMTEs with 1 day duration; b1–b2, EMTEs with 3 day duration;c1–c2, EMTEs with 5 day duration).

4.1.5 Changes of location centers of EMTEs

Figure 12 illustrates the projected locations of the centers of the severest EMTEs of different durations under the two warming scenarios. The black circle in Central China represents the center of the EMTE in the reference period. Under 1.5 ℃ warming, in addition to the center in the reference period, two new EMTE centers develop: one in North China around Beijing–Tianjin–Hebei and the other in

Southwest China around Chongqing–Sichuan. Under 2.0 ℃ warming, a fourth EMTE center develops in Xinjiang Province. Therefore, under global warming, additional centers of EMTE will appear, affecting a greater proportion of the population over a larger area.

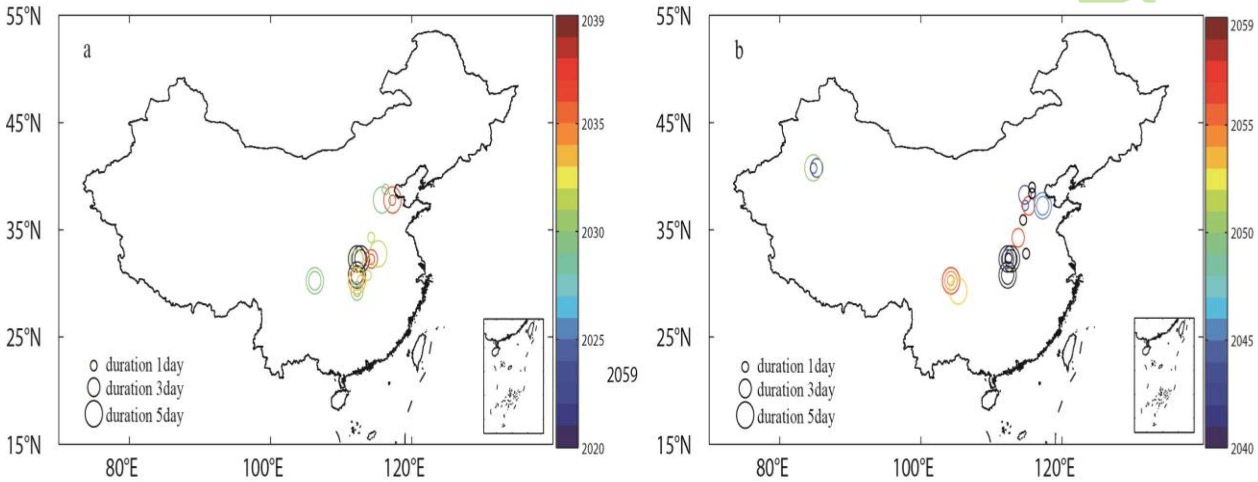

Fig. 12. Locations of maximum intensity centers of extreme maximum temperature events with different durations (a) under 1.5 warming and (b) under 2.0 ℃ warming.

4.2Population exposure to EMTEs

The severity of the impact of EMTEs depends not only on the events themselves but also on the levels of exposure and vulnerability. The level of exposure means the extent to which the adverse effects of EMTEs affect the population, economy, and other aspects (IPCC, 2012; 2014). It has been reported that increased exposure of a population to EMTEs leads to higher rates of mortality (Rey et al., 2009). The exposure of a population to an EMTE is defined as the population within the areal coverage of the event. Figure 13 illustrates the coverage and population exposure for every EMTE in the seven geographic areas of China defined in this study.

Coverage in the Northwest is large, but the population exposure is low because of the low population density. The exposure in Central China is the highest because of the large coverage and high population density. Table 1 shows the population exposed to 1–, 3–, and 5–day EMTEs under the reference period and 1.5 and 2.0 ℃ warming. Taking the 3–day EMTEs as an example, around 255.1 million people (20% of the total population) were exposed to EMTEs annually during the reference period. The population exposure was the largest in Central China, accounting for 35% of the total population exposure. The population exposure was smallest in Northeast and Northwest China, accounting for <3% of the total population exposure. Under 1.5 ℃ warming, it is projected that 338.6 million people would be exposed to 3–day EMTEs annually, an increase of 32.7% compared with the reference period. It is projected that the largest population exposure will remain in Central China and the smallest will be in Northeast and Northwest China. Under 2.0 ℃ warming, it is projected that 363.73 million people would be exposed to 3–day EMTEs annually, an increase of 7.4% compared with the 1.5 ℃ warming.

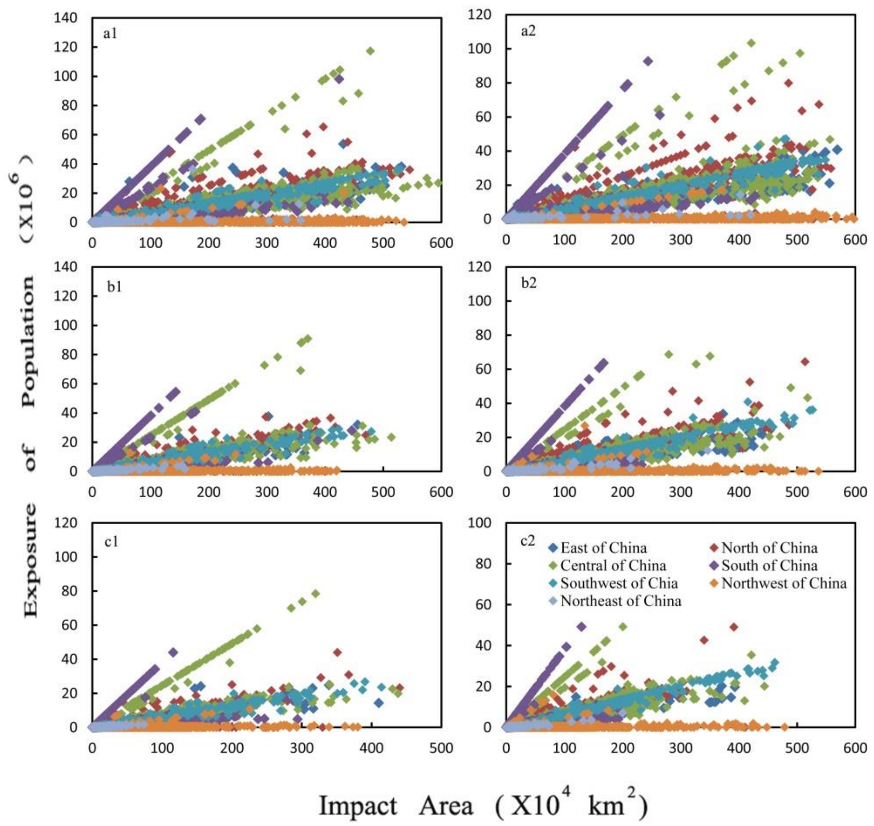

Fig. 13. Scatter plots of the population exposed to extreme maximum temperature events (EMTEs): (a1) 1–day EMTEs under 1.5°C warming, (b1) 1–day EMTEs under 2.0°C warming, (a2) 3–day EMTEs under 1.5°C warming, (b2) 3–day EMTEs under 2.0°C warming, (a3) 5–day EMTEs under 1.5°C warming, and (b3) 5–day EMTEs under 2.0°C warming.

Table 1. Number of people exposed to EMTEs 1986–2005, and under 1.5 and 2.0 ℃ warming (millions/a)

	1986－2005			Global Warming 1.5℃			Global Warming 2.0℃		
	1–day	3–day	5–day	1–day	3–day	5–day	1–day	3–day	5–day
Northeast China	3.40	1.44	0.73	3.70	1.69	0.97	2.46	2.42	1.45
North China	62.55	32.48	20.94	73.37	37.06	21.34	102.6	62.66	37.55
East China	66.30	46.01	35.54	73.79	52.54	40.30	76.23	58.58	44.19
Central China	129.6	89.39	62.05	160.1	123.8	96.55	132.1	108.9	86.15
South China	98.47	64.39	46.70	106.5	77.59	56.51	98.09	70.85	51.06
Southwest China	24.07	15.62	9.00	57.05	38.80	28.13	62.86	52.08	37.99
Northwest China	8.30	5.75	4.52	9.23	7.08	5.98	9.93	8.21	7.27
China	392.8	255.1	179.5	483.8	338.6	249.8	484.3	363.7	265.7

Figure14 and 15 show the rates of projected population exposure to 1–, 3–, and 5–day EMTEs, in different regions of China, under the 1.5 and 2.0 ℃ warming scenarios. In general, the population exposure is expected to increase under both warming scenarios; however, the rate of growth of the latter is higher than the former. Taking 3–day EMTEs as an example, it is projected that the population of China exposed to 3–day EMTEs will increase by 32.7% under 1.5 ℃ warming and by 42.6% under 2.0 ℃ warming. From a regional perspective, the Southwest China is projected to experience the fastest rate of growth of exposure, regardless of the magnitude of global warming. Under 1.5 ℃ warming, the rates of increase in population exposure in Central and South China are projected to be higher than under 2.0 ℃ warming. Conversely, the rates of increase under 2.0 ℃ warming are projected to be much higher in North, Northeast, and Northwest China than under 1.5 ℃ warming. This means that EMTEs might become more severe in northern China under the warmer scenario.

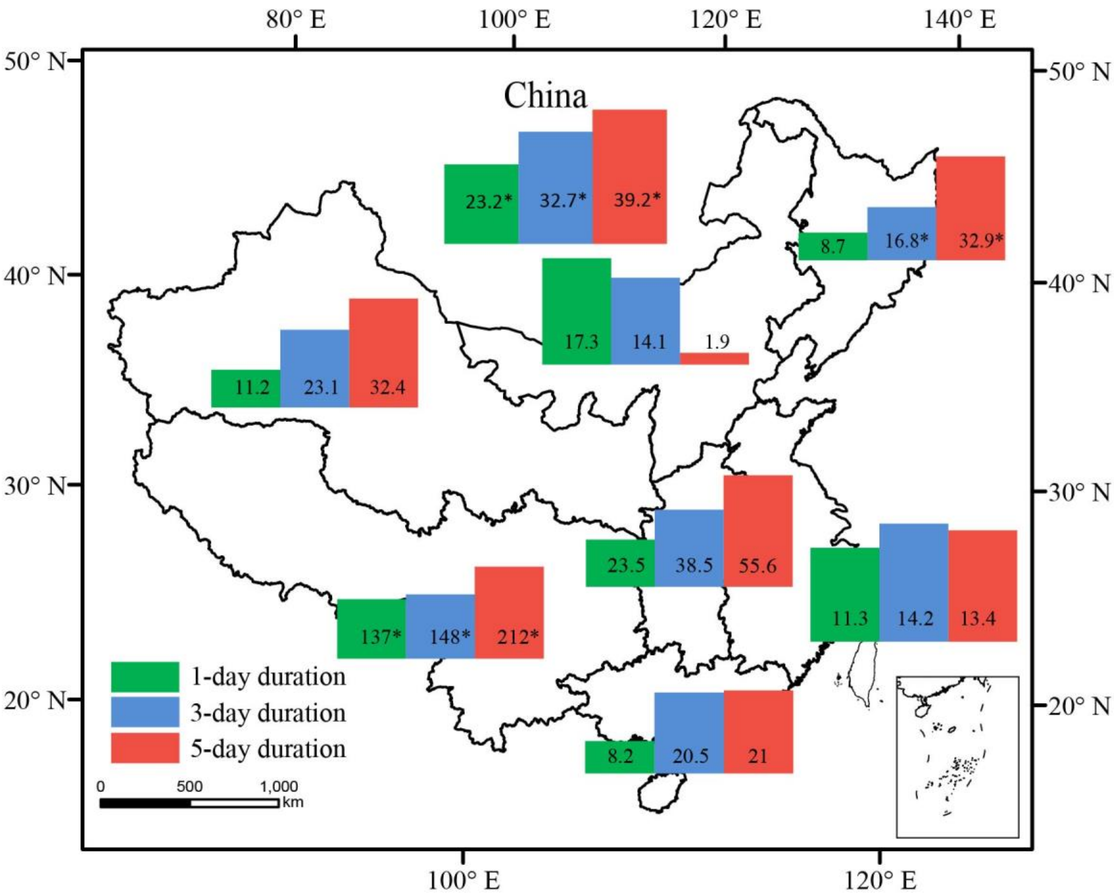

Fig. 14. Relative change (%) of number of people exposure to EMTEs under warming 1.5 ℃ (passing the 0.05 significance test).

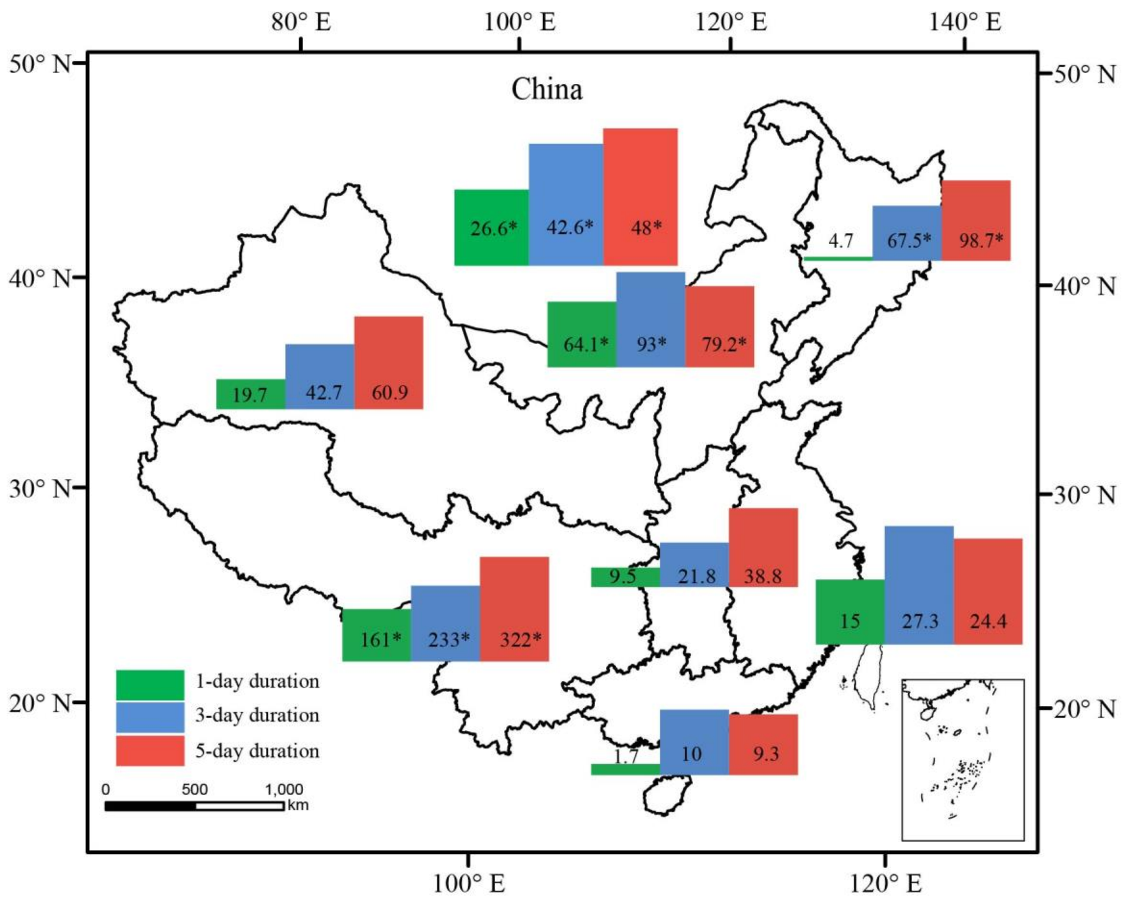

Fig. 15. Relative change (%) of number of people exposure to EMTEs under warming 2.0 ℃ (passing the 0.05 significance test).

5. Discussion

Global warming has already affected EMTEs in China during the 20th century, and continued warming could have further impact. In this study, we evaluated the simulation capability of the CCLM regional climate model by comparison with observational records from 756 metrological stations in China. It was determined that the CCLM was able to simulate satisfactorily the observed daily maximum temperature of the reference period (1986–2005) in China. Changes of frequency, intensity, and coverage of EMTEs under 1.5 and 2.0 ℃ global warming scenarios were presented based on the CCLM output. Furthermore, the exposure of the population of China to EMTEs in a warming world was projected based on 2010 demographic data.

With global warming, the frequency, intensity, and coverage of EMTEs are projected to increase and the greater the warming, the greater the increase. Table 2 presents the details of the frequency, intensity, and coverage of 1–, 3–, and 5–day EMTEs for the reference period and under the 1.5 and 2.0 ℃ warming scenarios. Under 1.5 ℃ warming, relative to the reference period, the number of EMTEs annually is projected to increase by 19–91, their intensity is projected to increase by 0.1–0.5 ℃, and their areal coverage is projected to increase by 0.54–0.72 million km^2. Under 2.0 ℃ warming, relative to the reference period, the number of EMTEs annually is projected to increase by 29–166, their intensity is projected to increase by 0.2–0.9 ℃, and their areal coverage is projected to increase by 0.88–1.24 million km^2. Compared with 1.5 ℃ warming, the number of EMTEs annually, their intensity, and area of impact under 2.0 ℃ warming increase by 10–75, 0.1–0.5 ℃, and 0.34–0.52 million km^2, respectively. Moreover, it should be noted that the frequency and coverage of longer–lasting EMTEs are projected to increase more than for EMTEs of shorter duration. This means that in a warmer future, longer–lasting EMTEs could become more severe. Some studies have found the same results. For instance, Schleussner (2015) estimated that for warming of 1.5 ℃, the global land area projected to experience heat waves would increase by 10% (0%–30%), and that the area of affected land would increase by 50% (30%–80%) under 2.0 ℃ warming.

Table 2. Frequency, intensity, coverage and population exposure of 1–day,3–day and 5–day EMTEs under Reference Period , Global Warming 1.5℃ and Global Warming 2.0℃

	Reference Period				Global Warming 1.5℃				Global Warming 2.0℃			
	A*	B*	C*	D*	A*	B*	C*	D*	A*	B*	C*	D*
1–day	1680	31.4	3.88	392.77	1699	31.5	4.60	483.84	1709	31.6	5.12	484.33
3–day	1490	32.6	2.48	255.08	1547	33.0	3.10	338.57	1595	33.5	3.51	363.73
5–day	1330	33.3	1.76	179.48	1421	33.8	2.30	249.78	1496	34.0	2.64	265.66

*(A=Frequency (times/a); B=Intensity (℃); C=Coverage (million km^2); D=Population Exposure (million/a))

Some EMTEs (regardless of whether 1–, 3–, or 5–day durations) for both warming scenarios are projected to be stronger than the severest events in the reference period. Under 1.5 ℃ warming, 10–24 unprecedented EMTEs might occur, whereas 26–72 unprecedented EMTEs might occur under 2.0 ℃ warming. Generally, a greater magnitude of global warming means a higher probability of the occurrence of unprecedented EMTEs. Diffenbaugh and Scherer (2011) found that even under the relatively moderate warming expected over the next half century, China is likely to experience unprecedented EMTEs. Therefore, it appears inevitable that China will face an increase in unprecedented EMTEs in the future.

The results of this study found there is always one center of severe EMTE in Central China during the reference period. Under 1.5 ℃ warming, there are two additional centers: one in the North and the other in the Southwest. Under 2.0 ℃

warming, a fourth center appears located in Xinjiang Region of China. The increasing number of centers of severe EMTEs means there will be a greater number of people and a larger area affected by the severest EMTEs in the future.

In a warming world, more people will be exposed to EMTEs, and the effects of EMTEs with wide spatial coverage and long duration on natural ecosystems and human health will be more severe. Under 1.5 and 2.0 ℃ warming, the population exposure is projected to increase by 70.3–91.07 and 86.18–108.65 million people/a, respectively, relative to the reference period. Compared with 1.5 ℃ warming, the population exposure increases by 0.49–25.16 million people /a under 2.0 ℃ warming. Population exposure increases with temperature, and new centers of the severest EMTEs are projected to appear around the Beijing–Tianjin–Hebei and Chongqing–Sichuan regions. Because of the dense population and developed economies of these areas, the effects of these new EMTEs will have even greater socioeconomic impact. Compared with 1.5 ℃ warming scenario, almost all the increase in population exposure under 2.0 ℃ warming is expected to take occur in North, Northeast, and Northwest China). The Northwest region of China in particular is an area in which the ecology is frail and the economy poorly developed. Under 2.0℃ warming, the impact of increasingly severe EMTEs could exacerbate this situation.

For China, the occurrence of unprecedented EMTEs appears inevitable in the future. However, the frequency, intensity, coverage, and population exposure of

EMTEs associated with 1.5 ℃ warming are lower than it with 2.0 ℃ warming. Furthermore, under 2.0 ℃ warming, northern China (especially the Northwest region) is expected to suffer relatively greater consequences associated with increasingly severe EMTEs. Based on the lesser of the two evils, it is recommended that the Chinese government do its utmost to achieve the goal of 1.5 ℃ warming.

Acknowledgments. We acknowledge the ISI–MIP coordination group at the Potsdam Institute of Climate Impact Studies in Germany for the provision of GFDL–ESM2M, HadGEM2–ES, IPSL–CM5A–LR, MIROCESM–CHEM, NorESM1–M, and MPI–ESM–LR data. We are grateful to Anqian Wang and Jinlong Huang of the University of the Chinese Academy of Sciences and to Jing Chen, Cheng Jing, and other graduate students for participating in this work. The authors are thankful for the constructive comments and suggestions by the editor and the reviewers.

References

Alexander, L.V., X. Zhang, T. C. Peterson, et al., 2006: Global observed changes in daily climate extremes of temperature and precipitation. *J. Geophys. Res.*, **111**, 1042–1063, doi: 10.1029/2005JD006290.

Andreadis, K. M., E.A. Clark, A.W. Wood, et al., 2005: Twentieth–century drought in the conterminous United States. *J. Hydrometeor.*, **6**, 985–1001, doi: 10.1175/JHM450.1.

Burkhard, R., W. Andreas, H. Andreas, et al., 2008: The regional climate model COSMO–CLM (CCLM). *Meteorologische Zeitschrift*, **17**, 347–348, doi: 10.1127/0941-2948/2008/0309.

Cao, L.G., J. Zhong, B.D. Su, et al., 2013: Probability distribution and projected trends of daily precipitation in China. *Adv. Clim. Change Res.*, **4**, 153–159, doi: 10.3724/SP.J.1248.2013.153.

Chen J., H.B. Liu, Y.J. Wang, et al., 2016: Variation of drought characteristics and its agricultural exposure in North China Plain. *Chinese J. Agrometeorology*, **37**, 587–599, doi: 10.3969/j.issn.1000-6362.2016.05.011. (in Chinese)

China Meteorological Administration, 2013. http://news.weather.com.cn/.

Dankers R., N.W. Arnell, D.B. Clark, et al., 2013: A first look at changes in flood hazard in the ISI–MIP ensemble. *Proc. Nat. Acad. Sci. USA*, **111,** 3257–3261, doi: 10.1073/pnas.1302078110/-/DCSupplemental.

Davie, J.C.S, P.D. Falloon, R. Kahana, et al., 2013: Comparing projections of future changes in runoff from hydrological and biome models in ISI–MIP. *Earth Sys. Dyn.*, **4**, 359–374, doi: 10.5194/esd-4-359-2013.

Diffenbaugh, N. S. and M. Scherer, 2011: Observational and model evidence of global emergence of permanent, unprecedented heat in the 20th and 21st centuries. *Climatic Change*, **107**, 615–624, doi: 10.1007/s10584-011-0112-y.

Ding, T., W. Qian, Z. Yan, 2010: Changes in hot days and heat waves in China during 1961–2007. *Int. J. Climatology*, **30**, 1452–1462, doi: 10.1002/joc.1989.

Ding, Y. H., G. Y. Ren, Z. C. Zhao, et al., 2007: Detection causes and projection of climate change over China: An overview of recent progress. *Adv. Atmos. Sci.*, **24**, 954–971, doi: 10.1007/s00376-007-0954-4.

Easterling, D.R., J. L. Evana, P.Y. Grosman, et al., 2000: Observed variability and trends in extreme climate events: A brief review. *Bull. Amer. Meteor. Soc.*, **81**, 417–425, doi: 10.1175/1520-0477(2000)081<0417:OVATIE>2.3.CO;2.

Easterling, D.R., B. Horton, P.D. Jones, et al., 2005: Maximum and minimum temperature trends for the globe: An update through 2004. *Science*, **32,** 364–367, doi: 10.1126/science.277.5324.364.

Field, C. B., V. Barros, T. F. Stocker, et al., 2012: Managing the risks of extreme events and disasters to advance climate change adaptation. Special report of the Intergovernmental Panel on Climate Change. *Journal of Clinical Endocrinology & Metabolism*, **18**, 586–599, doi: 10.1017/CBO9781139177245.012.

Fischer, T., C. Menz, B. D. Su, et al., 2013: Simulated and projected climate extremes in the Zhujiang river basin, South China, using the regional climate model COSMO–CLM. *J. Climatology*, **33**, 2988–3001, doi: 10.1002/joc.3643.

Frieler, K., R. Betts, E. Burke, et al., 2016: Assessing the impacts of 1.5 ℃ global warming–simulation protocol of the Inter–Sectoral Impact Model Intercomparison Project (ISIMIP2b). *Geoscientific Model Development*, **10,** 1-59, doi: 10.5194/gmd–2016–229.

Gemmer, M., T. Jiang, B.D. Su, et al., 2008: Seasonal precipitation changes in the wet season and their influence on flood/drought hazards in the Yangtze River Basin,China. *Quaternary International*, **186**, 12–21, doi: 10.1016/j.quaint.2007.10.001.

Greene, S., L. S. Kalkstein, D. M. Mills, et al., 2011: An examination of climate change on extreme heat events and climate–mortality relationships in large U.S. cities. *Wea. Climate Soc.*, **3**, 281–292, doi: 10.1175/WCAS-D-11-00055.1.

Hansen, J., M. Sato, R. Ruedy, et al., 2006: Global temperature change. *Proc. Nat. Acad. Sci. USA*, **103**, 14288–14293, doi: 10.1073/pnas.0606291103.

Homar, V., C. Ramis, R. Romero, et al., 2010: Recent trends in temperature and precipitation over the Balearic Islands. *Climatic Change*, **98**, 199–211, doi: 10.1007/s10584-009-9664-5.

Huang, J. L., H. Tao, T. Fischer, et al., 2015: Simulated and projected climate extremes in the Tarim river basin using the regional climate model CCLM. *Stoch. Environ. Res. Risk Assess.*, **29**, 2061–2071, doi: 10.1007/s00477-015-1059-8.

Huang, J. L., Y. J. Wang, T. Fischer, et al., 2017a: Simulation and projection of climatic changes in the Indus River Basin, using the regional climate model COSMO−CLM. *Int. J. Climatology*, **4**, 2545-2562, doi: 10.1002/joc.4864.

Huang, J. L., J. Q. Zhai, T. Jiang, et al., 2017b: Analysis of future drought characteristics in China using the regional climate model CCLM. *Climate Dynamics*, **10**, 1–19. doi: 10.1007/s00382–017–3623–z.

IPCC, 2012: *Managing the Risks of Extreme Events and Disasters to Advance Climate Change Adaptation.* United Kingdom and New York, NY, USA, Cambridge University Press, 326 pp.

IPCC, 2013: *Climate Change 2013: The Physical Science Basis.* Contribution of *Working Group I to the Fifth Assessment Report of IPCC the Intergovernmental Panel on Climate Change.* United Kingdom and New York, NY, USA, Cambridge University Press, 356 pp.

IPCC, 2014: *Climate Change 2014: Impacts, adaptation and vulnerability*. *Contribution of Working Group II to the Fifth Assessment Report of IPCC the Intergovernmental Panel on Climate Change*. United Kingdom and New York, NY, USA, Cambridge University Press, 569 pp.

Ito, A., K. Nishina, H.M. Noda. 2016: Impacts of future climate change on the carbon budget of northern high–latitude terrestrial ecosystems: An analysis using ISI–MIP data. *Polar Sci.*, 2016, **10,** 346–355, doi: 10.1016/j.polar.2015.11.002.

Jing, C., T. Jiang, Y.J. Wang, et al., 2016: A study on regional extreme precipitation events and the exposure of population and economy in China. *Acta Meteor. Sinica*, **74**, 572–582, doi: 10.11676/qxxb 2016.037. (in Chinese)

Karl, T. R., D.R. Easterling, 1999: Climate extremes: Selected review and future research directions. *Climatic Change*, **42**, 309–325, doi: 10.1023/A:1005436904097.

Kothawale, D.R., K.R. Kumar, 2005: On the recent changes in surface temperature trends over India. *Geophys. Res. Lett.*, **32**, 18714, doi: 10.1029/2005GL023528.

Kousari, M.R., H. Ahani, R. Hendi–Zadeh, 2013: Temporal and spatial trend detection of maximum air temperature in Iran during 1960–2005. *Global & Planetary Change*, **111**, 97–110, doi: 10.1016/j.gloplacha.2013.08.011.

Kruger, A.C., S.S. Sekele, 2013: Trends in extreme temperature indices in South Africa: 1962–2009. *Int. J. Climatology*, **33**, 661–676, doi: 10.1002/joc.3455.

National Bureau of Statistics of the People's Republic of China, 2010: The Sixth Nationwide Population Census Data. Available online at. http://www.stats.gov.cn/tjsj/tjgb/rkpcgb/qgrkpcgb/.

National Center for Health Statistics, 2007: National Vital Statistics System: Mortality data. Available online at. http://www.cdc.gov/nchs/deaths.htm.

National Weather Service, 2009: Weather fatalities. Available online at http://www.nws.noaa.gov/om/hazstats.shtml.

Perkins, S.E., L.V. Alexander, J. R. Nairn, 2012: Increasing frequency, intensity and duration of observed global heatwaves and warm spells. *Geophys. Res. Lett.*, **39**, 20714, doi: 10.1029/2012GL053361.

Qin N., J. Wang, G. Yang, et al., 2015: Spatial and temporal variations of extreme precipitation and temperature events for the Southwest China in 1960–2009. *Geoenvironmental Disasters*, **2,** 1–14, doi: 10.1186/s40677-015-0014-9.

Rey, G., A. Fouillet, P. Bessemoulin, et al., 2009: Heat exposure and socio–economic vulnerability as synergistic factors in heat–wave–related mortality. *European J. Epidemiology*, **24**, 495–502, doi: 10.1007/s10654-009-9374-3.

Rogelj, J.H., L.J. William, D.P. van Vuuren, et al., 2011: Emission pathways consistent with a 2 ℃ global temperature limit. *Nature Climate Change*, **1**, 413–418, doi: 10.1038/nclimate1258.

Schleussner, C.F., T.K. Lissner, E.M. Fischer, et al., 2015: Differential climate impacts for policy–relevant limits to global warming: the case of 1.5 ℃ and 2 ℃. *Earth Sys. Dyn. Disc.*, **6**, 2447–2505, doi: 10.5194/esdd-6-2447-2015.

Shi, Y.F., Y.P. Shen, D.L. Li, et al., 2003: Discussion on the present climate Change from warm–day to warm wet in northwest China. *Quaternary Sciences*, **23**, 152–164, doi:10.3321/j.issn:1001-7410.2003.02.005. (in Chinese)

Steppeler, J., G. Doms, U. Schättler, et al., 2003: Meso–gamma scale forecasts using thenon–hydrostatic model. *Meteor. Atmos. Phys.*, **82**, 75–96, doi: 10.1007/s00703-001-0592-9.

Sheffield, J., K.M. Andreadis, E.F. Wood, et al., 2009: Global and continental drought in the second half of the twentieth century: Severity–Area–Duration analysis and temporal variability of Large–Scale events. *J. Climate*, **22**, 1962–1981, doi: 10.1175/2008JCLI2722.1.

Su, B.D., J.L. Huang, M. Gemmer, et al., 2016: Statistical downscaling of CMIP5 multi–model ensemble for projected changes of climate in the Indus River Basin. *Atmos. Res.*, **178–179**, 138–149, doi: 10.1016/j.atmosres.2016.03.023.

Tan, F., B.D. Su, C. Gao, et al., 2012: High–resolution climate model(CCLM) for simulation of precipitation in the Huaihe River Basin,China. *Resour. Environ. in the Yangtze Basin*, **21**, 1236–1242. (in Chinese)

Thomson, A.M., K.V. Calvin, S.J. Smith, et al., 2011: RCP4.5: a pathway for stabilization of radiative forcing by 2100. *Climatic change*, **109**, 77–94, doi: 10.1007/s10584-011-0151-4.

United Nations Framework Convention on Climate Change (UNFCCC). 2015: The Paris Agreement. http://unfccc.int/paris_agreement/items/9485.php.

Upperman, C.R., J. Parker, C. Jiang, et al., 2015: Frequency of extreme heat event as a surrogate exposure metric for examining the human health effects of climate change. *Plos One*, **10**, 1–15, doi:10.1371/journal.pone.0144202.

Valleron, A. J., A. Boumendil, 2004: Epidemiology and heatwaves: Analysis of the 2003 episode in France. *Comptes Rendus Biologies*, **327**, 1125–1141, doi: 10.1016/j.crvi.2004.09.009.

Vuuren, D.P.V., J. Edmonds, M. Kainuma, et al., 2011: The representative concentration pathways: an overview. *Climatic Change*, **109**, 5, doi: 10.1007/s 10584–011–0148–z.

Vescovi, L., A. Bourque, G. Simonet, et al., 2009: Transfer of climate knowledge via a regional climate–change management body to support vulnerability, impact assessments and adaptation measures. *Climate Research*, **40** 163–173, doi: 10.3354/cr00787.

Wang, D., C. Menz, T. Simon, et al., 2013: Regional dynamical downscaling with CCLM over East Asia. *Meteor. Atmos. Phys.*, **121**, 39–53, doi: 10.1007/s00703-013-0250-z.

Wang, P.X., J.H. Yang. 2007: Extreme high temperature events and response to regional warming in recent 45 years in Northwest China. *J. Desert Res.*, **27**, 649–655.

Warszawski, L., K. Frieler, V. Huber, et al., 2014: The Inter–Sectoral Impact Model Intercomparison Project (ISI–MIP): Project framework. *Proc. Nat. Acad. Sci. USA*, **111**, 3228–32, doi: 10.1073/pnas.1312330110.

Xu, Y., X.J. Gao, Y. Shen, et al., 2009: A daily temperature dataset over China and its application in validating a RCM simulation. *Adv. Atmos. Sci.*, **26**, 763–772.

Zhai, J.Q., J.L. Huang, B.D. Su, et al., 2017: Intensity–Area–Duration analysis on droughts in China. *Climate Dynamics*, **48,** 151-168, doi: 10.1007/s00382–016–3066–y.

Zhang, S.Y., S.R. Wang, Y.S. Zhang, et al., 2004: The climate character of high temperature and the prediction in the large cities of east of China. *J. Tropical. Meteor.*, **20**, 750–760.

Zhang, F., H. Gao, X. Cui., 2008: Frequency of extreme high temperature days in China, 1961–2003. *Weather*, **63**, 46–49, doi: 10.1002/wea.136.

Zhou Y., G.Y. Ren. 2011: Change in extreme temperature event frequency over mainland China, 1961−2008. *Climate Research*, **50,** 125–139, doi: 10.3354/cr01053.